PROCEEDINGS, TOUGH Symposium 2003
Lawrence Berkeley National Laboratory, Berkeley, California, May 12–14, 2003

SCALING OF HOT BRINE INJECTION WELLS: SUPPLEMENTING FIELD STUDIES WITH REACTIVE TRANSPORT MODELING

Yvette Ontoy[1], Phil Molling[2], Tianfu Xu[3], Nicolas Spycher[3], Mauro Parini[2], and Karsten Pruess[3]

[1] *Philippine Geothermal, Inc., Makati City, Philippines - yvette.ontoy@unocal.com*
[2] *Unocal, Geothermal Technology & Services, Santa Rosa, CA - pmolling@unocal.com*
[3] *Lawrence Berkeley National Lab, Berkeley, CA - TianFu_Xu@lbl.gov*

ABSTRACT

Hot brine injector Naglagbong-67 (Nag-67) located in the Tiwi Geothermal Field, Philippines had been in operation for over ten years when injectivity decline indicated a workover was required in 2000. The workover consisted of drilling out wellbore scale followed by acid dissolution of scale formed in the near-wellbore formation. The scale drillout improved the injection capacity of the well from a pre-workover value of 3.8 kg/s to 25.2 kg/s. The acid stimulation further increased the capacity to near its initial-use capacity of 113.4 kg/s. These results, as well as scale-volume estimates from brine chemistry and from stoichiometric amounts of silica dissolved during the acidizing, suggested that the decrease in injection capacity of the well was largely due to scale deposition in the near-well formation.

To understand the scaling process and loss of injectivity in hot brine injectors, factors that cause the deposition of amorphous silica in the near-well formation were identified and the extent of their effect was simulated using the reactive geochemical transport modeling tool TOUGHREACT. A radial, one-dimensional model of the formation around the bottommost permeable zone of Nag-67 was used and constrained with reservoir data, the mineralogy of the host rock, and the average composition of the brine being injected. A sensitivity study was performed to determine which among the identified factors were most likely to affect silica deposition. Simulation results were compared with actual measured injection data and correlated with historical events.

INTRODUCTION

This paper reports on field studies and preliminary numerical analyses carried out to understand scaling mechanisms in an injection well, Naglagbong-67 (Nag-67), at the Tiwi Geothermal Field, Philippines. The objective of this work was to integrate analyses of field data and reactive transport modeling in an effort to improve the planning of injection operations in such a way as to minimize injectivity loss from scaling.

In the Tiwi Geothermal Field, steam that is used for power generation is separated from a two-phase fluid produced from the wells. Since 1993 all separated brine has been injected at reservoir depths in several groups of edgefield and outfield wells that were found to have minimal impact on production (Santos and Carandang-Racela, 1993).

Brine normally contains chemical components that potentially can deposit scale at some optimal condition. Among potential scaling species, silica has proved to be the most common due to its high concentration in geothermal fluids and its temperature-dependent solubility. The long pipelines commonly required to reach injection well locations exacerbate the problem by increasing residence time and cooling of the brine. Operation of hot brine injection systems at relatively low flow conditions can also lead to flashing, that further enriches silica in the brine and localizes scaling.

Scaling in injection wells causes decline in their injection capacity. Loss of injection capacity could lead to generation loss, as production from two-phase wells would need to be curtailed to comply with zero discharge policies. Scale cleanouts are usually done to recover lost capacity of injectors.

The timing and mechanism of scaling, however, remains enigmatic. The injected hot brine is typically close to saturation with respect to amorphous silica. As injectate re-enters the hotter host rock of the permeable zone, the scaling rate and saturation lowers. Understanding the mechanism of scaling is critical to mitigating the loss of injectivity.

ANALYSES OF FIELD DATA

Nag-67 is one of the hot brine injectors located to the south-east of the Tiwi production field. The well was completed in March 1987 as a deviated hole with the 9 5/8" casing shoe set at 917 m MD (Measured Depth), and the top of the 7" production liner at 878 m MD with the shoe at 2114 m MD (1873 m TVD - Total Vertical Depth).

Records of injection history (Figure 1) and fluid chemistry for Nag-67 were reviewed to determine the

nature of deposited scale and to estimate the amount and location of scale deposition. This semi-quantitative analysis provided a basis from which numerical analyses could then be carried out.

Analysis of Injection Records

The well was acidized in January 1989 primarily to clear the near-wellbore formation of drilling mud damage and to improve its injectivity. Injection capacity of the well after the stimulation was 126 kg/s at a wellhead pressure of 1.38 MPa. In 1996, the well was found to accept only 38 kg/s at an injection wellhead pressure of about 1.0 MPa. Decrease in injection capacity was attributed to scaling inside the wellbore because as early as October 1992, the liner was found reduced in diameter to 5" at the depth of 1651 m. In 1999, an injectivity test indicated the capacity of the well reduced to 17 kg/s at an injection wellhead pressure of 1.31 MPa. In March 2000, recorded injection in Nag-67 suddenly dropped to 3. 8 kg/s.

In January 2001, scale inside the Nag-67 wellbore was drilled-out and the scale deposited in the near-well formation was dissolved by acid. Measurements after the scale drillout indicated that the capacity of the injector went up to 25.2 kg/s, and another test after the acid stimulation showed a further increase to 113.4 kg/s. These results strongly suggested that the decline in injectivity of the well was caused primarily by scale deposition in the near-well formation.

Based on the chemistry of the brine injected and analysis of some scale deposited, the majority of scale in Nag -67 was determined to be amorphous silica.

Estimated Scale Amount and Location

The SiO_2 concentration and pH of brine being supplied to the Nag-67 injector were monitored between 1989 and 2000. Complete brine analyses were also available for every year except 1999 and were used to characterize the saturation state of the brine with respect to other minerals. Only SiO_2 polymorphs were found to be saturated or supersaturated. On average, the brine contains 690 ppm SiO_2 and has a pH of 6.4. The range of values of measured SiO_2 in solution is 530 to 800 ppm and the pH ranges from 5.4 to 7.6.

From this historical chemical record, the degree of amorphous silica saturation in each analyzed water sample was determined (as ppm SiO_2 above the amorphous silica solubility at the temperature of the sampled brine). Two sources were initially considered for the amorphous silica solubility (SUPCRT92, Johnson et al., 1992; Gunnarsson and Arnorson, 2000). The latter source was deemed the best currently available (note that differences in solubilities reported in these two sources are less than the solubility change associated with the range of measured temperatures of the injectate, 152-170°C). Using the data of Gunnarsson and Arnorsson (2000) for amorphous silica solubility, the average degree of supersaturation in the injected brine over time was estimated to be around 10 ppm (as SiO_2), and ranging between –100 ppm (i.e., undersaturated) and +200 ppm. A supersaturation by 10 ppm SiO_2 was calculated to correspond to a typical brine temperature of 160°C.

By multiplying the total volume of brine injected with the average silica supersaturation value of 10

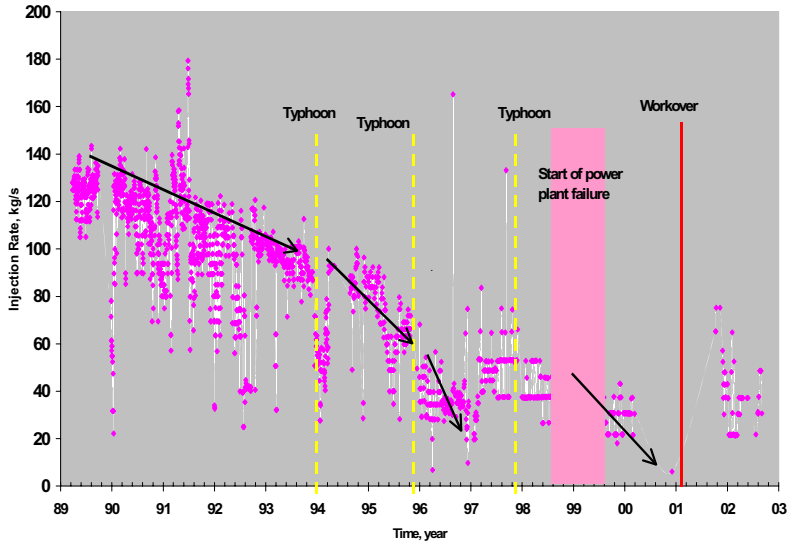

Figure 1. Historical injection rates (kg/s) in Nag-67.

ppm, the amount of silica that could potentially have deposited inside the wellbore and in the formation from 1989 to 2001 was estimated to be 55.4 m^3. Records of the well drillout and acidification were then used to estimate how much of this scale could have deposited inside the wellbore (as opposed to formation). Pre-drillout sinker bar diameter runs helped to describe the location and thickness of scale in the wellbore. Using the description of returns, drilling rate and return rates, a "best guess" of the location and thickness of the scale was made. An important observation came from this analysis. The bottommost entry must have been mostly open to drilling fluid because no fluid returned to the surface once the scale in the wellbore was cleared. This suggests that the bottommost permeable zone was reconnected to the wellbore. Volume calculations based on the likely geometry of scale indicated that half of the total scale amount could have been deposited in the wellbore and annulus (27 m^3). A large amount (28.5 m^3) of scale, then, could have been deposited in the formation (Table 1).

Table 1. Estimates of potential scale volume.

Scale Calculation Type	*Volume, m^3*
Total scale potential in brine (10 ppm SiO_2 in solution)	55.4
Potential scale inside the well and annulus	27.0
Potential scale in the formation	28.5
Maximum scale in the formation dissolved by acid	1.4

The estimated amount of silica (in the formation) dissolved by acid stimulation was then calculated by assuming that the acid chemical used dissolved a stoichiometrically equivalent amount of silica. The silica scale volume calculated in this way is only 1.4 m^3. The dissolution of this seemingly small amount of amorphous silica, nevertheless increased the injection capacity of the well to near original capacity. Therefore, it would appear that in the present case, a significant part of the injectivity loss was related to silica deposition in the formation close to the wellbore, as opposed to in the wellbore itself. For this reason, further work was conducted to evaluate factors leading to silica deposition in the formation around the injection well. These factors and the extent of their effect were evaluated using the non-isothermal multi-component reactive fluid flow and geochemical transport code TOUGHREACT (Xu and Pruess, 1998 and 2001), as discussed below.

NUMERICAL ANALYSES

Main Features of Numerical Model

The numerical simulation tool TOUGHREACT was developed by introducing reactive chemistry into the framework of the existing multi-phase fluid and heat flow code TOUGH2 (Pruess, 1991) in which the flow and transport in geologic media are based on space discretization by means of integral finite differences (Narasimhan and Witherspoon, 1976). An implicit time-weighting scheme is used for the individual components of the model consisting of flow, transport, and geochemical reaction. TOUGHREACT uses a sequential iteration approach, which solves the transport and the reaction equations separately. The system of chemical reaction equations is solved by a Newton-Raphson iterative method similar to that of Parkhurst (1980), Reed (1982), and Wolery (1992). Full details on numerical methods are given in Xu and Pruess (1998 and 2001). The model can accommodate any number of chemical species present in liquid, gas and solid phases.

The model can be applied to one-, two-, or three-dimensional porous and fractured media with physical and chemical heterogeneity. The model can accommodate any number of chemical species present in liquid, gas and solid phases. A wide range of subsurface thermo-physical-chemical processes is considered. Major processes for fluid and heat flow are: (1) fluid flow in both liquid and gas phases occurs under pressure and gravity forces; (2) capillary pressure effect for the liquid phase; (3) heat flow by conduction, convection and diffusion. Transport of aqueous and gaseous species by advection and molecular diffusion is considered in both liquid and gas phases. Aqueous chemical complexation and gas dissolution/exsolution are considered under the local equilibrium assumption. Mineral dissolution and precipitation can be modeled with TOUGHREACT either subject to local equilibrium or kinetic conditions.

In the present version of TOUGHREACT, the following processes are neglected: (1) compaction and thermal mechanics, such as micro-fracturing by thermal stress and hydro-fracturing by thermal expansion of pore fluid; (2) the effect of chemical concentration changes on fluid thermophysical properties such as density and viscosity which are otherwise primarily dependent on pressure and temperature; (3) the enthalpy due to chemical reactions.

Reaction Rates

For kinetically-controlled mineral dissolution and precipitation, a general form of the rate law (Steefel and Lasaga, 1994) is used

$$r_m = \pm k_m A_m \left| \left[\left(\frac{Q_m}{K_m} \right)^{\mu} - 1 \right] \right|^n \qquad (1)$$

where m is mineral index, $\mathbf{r}_m$ is the dissolution/precipitation rate (positive values indicate dissolution, and negative values precipitation), $\boldsymbol{A}_m$ is the specific reactive surface area per kg H_2O, $\boldsymbol{k}_m$ is the rate constant (moles per unit mineral surface area and unit time) which is temperature dependent, $\boldsymbol{K}_m$ is the equilibrium constant for the mineral-water reaction written for the destruction of one mole of mineral m, $\boldsymbol{Q}_m$ is the ion activity product, the exponents μ and n are two positive numbers normally determined by experiments, and are usually, but not always, taken equal to unity (as in the present work).

A somewhat different rate law is used for the precipitation of amorphous silica (modified from Carroll et al., 1998), as follows:

$$r_m = k_m A_m \left[\left(Q/K \right)^{4.4} - \frac{1}{\left(Q/K \right)^{8.8}} \right] \qquad (2)$$

with parameters as defined for Equation 1.

The temperature dependence of the reaction rate constant can be expressed reasonably well via an Arrhenius equation (Steefel and Lasaga, 1994) as follows:

$$k = k_{25} \exp\left[\frac{-E_a}{R} \left(\frac{1}{T} - \frac{1}{298.15} \right) \right] \qquad (3)$$

where E_a is the activation energy, k_{25} is the rate constant at 25°C (k_0 in Eq. 2), R is the gas constant, and T is the absolute temperature.

The effect of changing pH (from values pH_o to pH) on reaction rates is taken into account by the relationship:

$$\log(\mathbf{r}_m)_{pH} = \log(\mathbf{r}_m)_{pHo} + slope\ (\text{pH-pH}_o) \qquad (4)$$

where *slope* is the slope of $\log(\mathbf{r}_m)$ change with pH. This essentially correspond to multiplying the reaction rate by a factor related to the activity of hydrogen ion raised to some exponent equal to *slope*. In this study, the effect of pH on reaction rate was considered only for amorphous silica precipitation (i.e. *slope* = 0 for all other minerals). Using a typical pH range of 5.0–7.0, and silica deposition rates as a function of pH, the precipitation rate of amorphous silica (in logarithmic form) was found to follow approximately a linear trend with pH, with a positive slope around 0.7. Therefore, for amorphous silica only, the slope in Eq. 4 was set to 0.7 (and pH_o arbitrarily set to 7).

Porosity and Permeability Change

Temporal changes in porosity and permeability due to mineral dissolution and precipitation can modify fluid flow. This feedback between flow and chemistry is considered in our model. Changes in porosity during the simulation are calculated from changes in mineral volume fractions. For porous media, a simple Kozeny-Carman grain model based on spheres can be used to calculate changes in permeability due to changes in porosity. The Kozeny-Carman equation relates the permeability **k** (in m^2) to the porosity ($\boldsymbol{\phi}$) by

$$k = \frac{R_0^2}{45} \left(\frac{\phi^3}{(1-\phi)^2} \right) \qquad (5)$$

where R_0 is the initial local spherical close pack radius. Hence, the ratio of the permeability **k** to initial permeability $\mathbf{k}_0$ can be expressed as

$$\frac{k}{k_0} = \left(\frac{\phi}{\phi_0} \right)^3 \left(\frac{1-\phi_0}{1-\phi} \right)^2 \qquad (6)$$

where $\boldsymbol{\phi}_0$ is the initial porosity.

Although this relationship was used in the present study, it was recognized that it may not be best suited for fractured rock. For this reason, an alternative relationship that may be more applicable to fractures and has a larger permeability drop for a smaller decrease in porosity is considered later.

Mesh Setup and Fluid Flow Parameters

The formation region at the bottommost permeable zone of Nag-67 was modeled. This zone extends over a thickness of 120 m. A simple one-dimensional radial flow model was used, consisting of 50 radial blocks with logarithmically increasing radii (Figure 2).

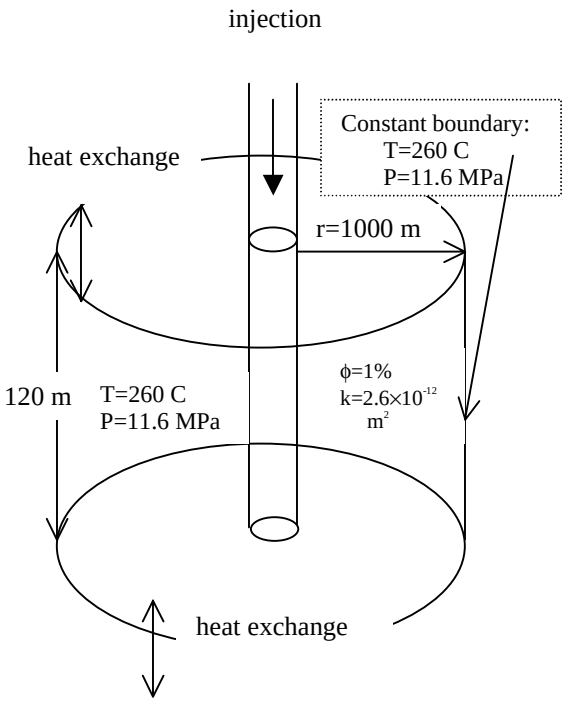

Figure 2. Simplified conceptual model for injection well Nag-67.

The 50 blocks represent a distance of 1000 m from the outer edge of the drilled open hole. Only the fracture network (assumed to represent 1% of the total formation volume) is considered in the model, with the assumption that the fluid exchange with the surrounding low permeability matrix is insignificant. To allow for chemical reaction with the rock, a 50% porosity was assigned to the blocks, and the total volume was accordingly doubled. The modeled zone was therefore "compressed" into a 2.4 m thick layer with 50% pore volume and 50% rock volume. A permeability of 2.6×10^{-12} m^2 was used, corresponding to a bulk fracture permeability value of 2.6×10^{-14} m^2 for the whole formation thickness with 1% fracture porosity. Initial reservoir temperature and pressure used were 260°C and 11.6 MPa, respectively. Heat transfer between fracture and matrix was accounted for by allowing heat exchange with assigned confining layers.

The injection history of the well was used to define the amount of injected mass versus time: 50% of the total injection rate in Nag-67 was assigned to the bottommost permeable zone because spinner surveys showed that the zone accepted 50% of the injectate. Injectate was assumed to come from a point source in the middle of the innermost block.

Input Geochemical Data

The types and initial abundances of primary minerals were determined from the reported Nag-67 alteration mineralogy at the 1798-1920 m MD permeable zone (propylitic/phyllic rock). Secondary minerals were also determined from field observations (Table 2).

Table 2. Minerals and Aqueous Species Considered in Simulations

Mineral	Mineral Precipitation /Dissolution	Mineral Initial Volume fraction	Primary Aqueous Components
Primary:			
albite-low	Kinetic	0.18	H_2O
anorthite	Kinetic	0.02	H^+
illite	Kinetic	0.05	Ca^{+2}
quartz	Kinetic	0.14	Mg^{+2}
muscovite	Kinetic	0.16	Na^+
clinochlore-7a	Kinetic	0.08	Cl^-
clinozoisite	Kinetic	0.01	$SiO_{2(aq)}$
calcite	Equilibrium	0.13	HCO_3^-
			SO_4^{-2}
Secondary:			K^+
amorphous silica	Kinetic		AlO_2^-
microcline	Kinetic		
kaolinite	Kinetic		
anhydrite	Equilibrium		

The composition of the injected brine was provided from historical analytical data. The formation water was reconstituted from the known brine composition as follows. First, the brine was numerically diluted to yield saturation with quartz at the observed reservoir temperature of 260°C (thus reversing the concentrative effect of flashing). The resulting water was then equilibrated with minerals identified in the well mineralogy log (calculating the aluminum concentration using equilibrium with microcline, sodium using albite, pH using calcite, calcium using clinozoisite, and magnesium using clinochlore). Calcite and anhydrite were assumed to react at equilibrium because their reaction rate is typically quite rapid. Other minerals were set to react under kinetic constraints (Table 2). Thermodynamic and kinetic data for amorphous silica were taken from Gunnarsson and Arnorsson (2000) and Carroll et al., (1998), as mentioned earlier. For other minerals, thermodynamic and kinetic data were taken from various other literature sources.

For all minerals except amorphous silica, input surface areas were estimated from the geometric surface area of the modeled fracture (around 130 $m^2/m^3_{\text{fractured medium}}$). For amorphous silica, a large surface area was estimated (10^7 cm^2/g) from Parks (1990, Fig. 16). Such a large value takes into account

the very small size that amorphous silica particles can have in solution.

Sensitivity Analyses

Factors that were identified to possibly have an effect on scale formation are 1) the silica concentration in the hot brine injectate, 2) the temperature of the injectate, 3) the flowrate of the injectate, 4) the pH of the injectate, and 5) the temperature and pressure conditions of the reservoir in the vicinity of the injector.

A number of simulations were performed to test how these factors affect scale formation. Simulations were carried out for ten years of continuous injection. Table 3 shows the range of values tested for each input parameter and the actual range of observed values for each.

Table 3. Sensitivity analyses.

Variable	*Value Range*	
	Field Observations	*Modeled*
Silica concentration in hot brine, ppm	530 – 800	708- 852
Temperature of injectate	152 – 171 $^{\circ}C$	152 – 171 $^{\circ}C$
Temperature of reservoir rock	232 – 288 $^{\circ}C$	232 – 288 $^{\circ}C$
Pressure of reservoir rock	11.72 – 13.44 MPa	11.72 – 13.44 MPa
Flowrate of injectate	3. 8 – 113.4 kg/s	3. 8 – 100.8 kg/s
pH of injectate	4 – 7	5 – 7

Simulation Results

Simulation results indicate that amorphous silica is by far the most abundant mineral to precipitate upon injection of the brine. For this reason, and because these results corroborate observations from analyses of scale samples, the precipitation or dissolution of minerals other than amorphous silica is not discussed here.

Examples of results are presented for three simulations, each using a different injection temperature (152, 160, and 171°C), but the same SiO_2 concentration in the injected brine (752 ppm) and same initial reservoir temperature (260°C) (Figures 3, 4 and 5). As would be expected, the maximum amount of amorphous silica precipitates at the lowest injectate temperature of 152°C (Figure 3). At this temperature, the silica concentration in the brine (752 ppm) exceeds the solubility of amorphous silica by approximately 100 ppm. At 160°C, the solubility of amorphous silica is exceeded by 50 ppm and, accordingly, less silica is precipitated. At 171°C, the brine is undersaturated with respect to amorphous silica (by 16 ppm) and no silica is precipitated (thus no curve is shown for this temperature on Figure 3).

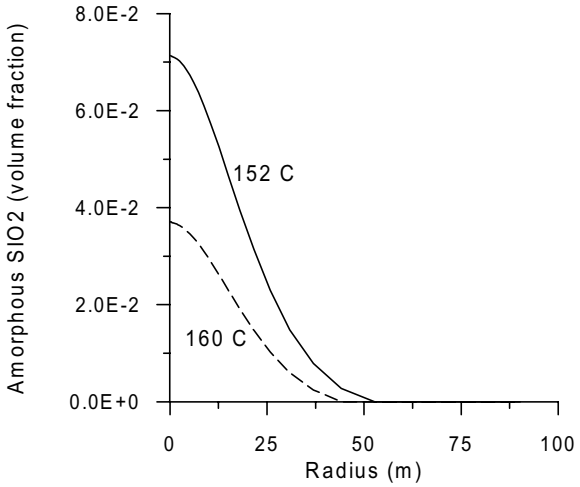

Figure 3. The precipitation of amorphous silica (in volume fraction) after 10 years. (No amorphous silica existed in the model at initial-state).

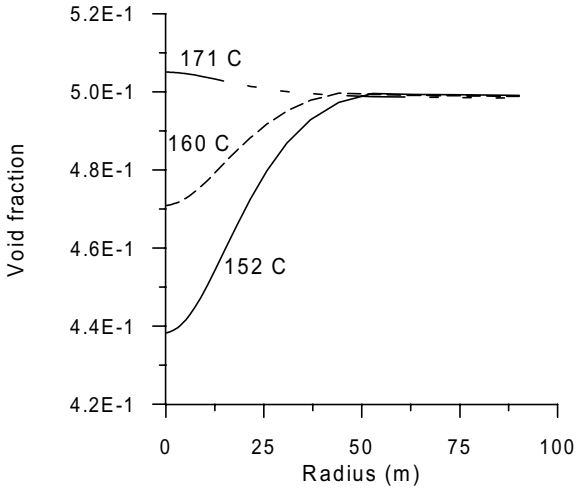

Figure 4. Void fraction after 10 years at three injectate temperatures. Initially, the model has an assigned void fraction of 50% (see text).

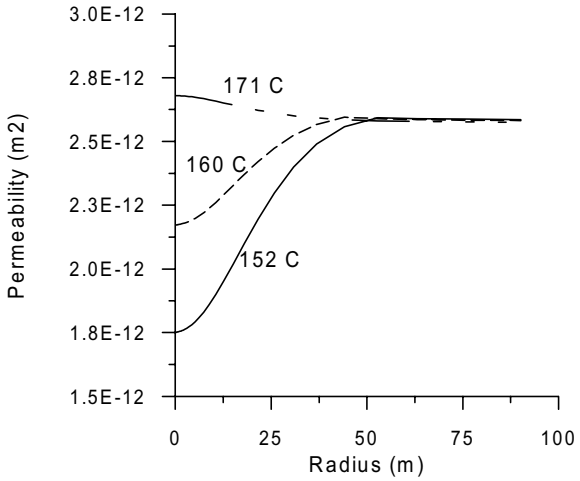

Figure 5. Permeability distribution after 10 years (calculated using Equation 6)

The precipitation of amorphous silica is predicted to take place within the first 50 meters (horizontally) from the injector (Figure 3). Accordingly, predicted changes of porosity (Figure 4) and permeability (Figure 5) are limited to a zone extending approximately 50 meters from the injection point.

At the higher investigated temperature (171°C), the porosity and permeability slightly increase from the dissolution of primary minerals, because the brine is undersaturated with respect to these minerals and amorphous silica. At lower temperatures, the precipitation of amorphous silica results in a decrease in fracture void volume, by up to 12% at 152°C (Figure 4). The corresponding permeability decrease is about 30% (Figure 5) because of the weak coupling between porosity and permeability provided by Equation 4 (the effect of a stronger coupling is evaluated later).

Results of the various sensitivity analyses are summarized in Table 4. The increase in silica deposition with increasing pH is directly related to the effect of pH on the amorphous silica precipitation rate, as described earlier.

DISCUSSION

The scale drillout records and the success of the acid stimulation showed that the loss of injectivity of the well was caused primarily by scale deposition in the formation close to the wellbore. On the other hand, simulations showed only a modest permeability decrease, even assuming the lowest temperature values (see Figure 5). This is inconsistent with the observed dramatic loss of injectivity. For this reason, another simulation was also performed using a brine with a temperature of 152°C and a silica concentration to 852 ppm (200 ppm above the solubility of amorphous silica) for ten years of continuous injection. This was deemed a worst possible scenario, using 20 times what is considered the average silica supersaturation of the injectate, and approximately the highest silica concentration ever measured in the brine. This simulation still underestimated the actual drop in permeability and injectivity of the well.

The likely major reason of not capturing permeability drop and injectivity loss is that the simple cubic Kozeny-Carman porosity-permeability equation cannot reflect complex relationship of porosity and permeability in geologic media that depends on a interplay of many factors, such as pore size distribution, pore shapes, and connectivity (Verma and Pruess, 1988). Laboratory experiments have shown that modest reductions in porosity from mineral precipitation can cause large reductions in permeability (Vaughan, 1987). Detailed analysis of a large set of field data also indicated a very severe dependence of permeability on small porosity changes (Pape et al., 1999). This is explained by the convergent-divergent nature of natural pore channels, where pore throats can become clogged by precipitation while disconnected void spaces remain in the pore bodies (Verma and Pruess, 1988). The permeability reduction effects depend not only on the overall reduction of porosity but also on details of the pore space geometry and the distribution of precipitate within the pore space. These may be quite different for different media, which makes it difficult

Table 4: Results of sensitivity analyses

Parameter Varied (See Table 2 for range)	*Fixed Conditions*	*Results*
Silica concentration in hot brine	Temperature of injectate: 160°C Temperature of reservoir: 260°C	Strong control on silica deposition (for supersaturated conditions). High concentration leads to high porosity drop.
Temperature of injectate	Silica concentration: 752 ppm Temperature of reservoir: 260°C	Strong control on silica deposition. Decrease in temperature leads to significant drop in porosity.
Temperature and pressure of reservoir rock	Temperature of injectate: 160°C Silica concentration: 752 ppm	Negligible effect on precipitation of silica and on porosity drop (at modeled reservoir rock temperatures higher than the injected brine temperature).
Flowrate of injectate	Temperature of injectate: 160°C Silica concentration: 752 ppm	Strong control on silica deposition. Low rates leads to deposition near the wellbore. High rates leads to more distal deposition.
pH of injectate	Temperature of injectate: 160°C Silica concentration: 752 ppm	Strong control on silica deposition. Increasing pH leads to increasing porosity drop.

to achieve generally applicable predictions. To evaluate the effects of a more sensitive coupling of permeability to porosity than the Kozeny-Carman relationship (Eq. 6), we also investigated an improved porosity-permeability relationship presented by Verma and Pruess (1988)

$$\frac{k}{k_0} = \left(\frac{\phi - \phi_c}{\phi_0 - \phi_c} \right)^n \qquad (7)$$

where ϕ_c is the value of "critical" porosity at which permeability goes to zero, and n is a power law exponent. Parameters ϕ_c and n are medium-dependent. Here, we arbitrarily chose $\phi_c = 0.42$ and n = 1.5. Taking porosity values from Figure 4 and using Eq. (7), the corresponding permeability decrease close to the borehole is calculated to be about one order of magnitude (Figure 6). Therefore, by using such a relationship instead of Eq. (6), the match between observed and simulated injection rates and pressures could be improved. However, to implement Eq. (7) into the numerical simulations, further studies would be required to calibrate parameters ϕ_c and n to field data. The authors plan to further investigate the effect of alternative porosity-permeability relationships.

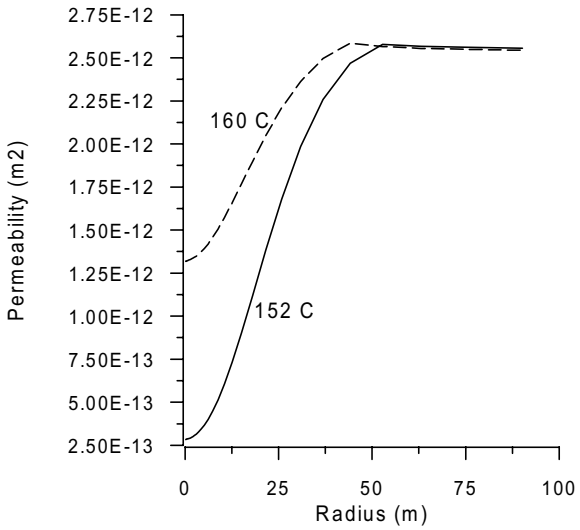

Figure 6. Permeability distribution after 10 years (calculated using Equation 7)

If the second relationship is considered to be more appropriate for fractured media, then it is possible that continuous injection of slightly over-saturated brine could account for the injectivity loss of Nag-67. However, a review of the injection history also shows increased rates of injectivity loss after prolonged shutdowns caused by typhoons (Figure 1). It is therefore possible that such interruptions in operation could also be a significant cause of the loss of injectivity. During these times, the flow of brine in the pipelines, in the well, and through the well annulus may be greatly reduced, thus lengthening the residence time of the brine and enhancing silica deposition. The effect of residence time on amorphous silica precipitation has been most recently demonstrated in laboratory experiments reported by Icopini et al. (2002). Increased residence time would allow silica to form longer chains, thereby increasing the scaling potential. These particular mechanisms of silica precipitation, including nucleation thresholds, are not currently incorporated into TOUGHREACT. Nevertheless, the kinetic formulation of amorphous silica precipitation (Eq. 2) captures the general relationship of time with silica deposition at various flow rates. Therefore, the current model could be used for further sensitivity analyses to evaluate silica precipitation during (1) periods of time when spikes in silica concentration occur and (2) the intermittent periods when brine is left in a "nearly-stagnant" condition in the wellbore and in the rock formation around the injection well.

CONCLUSIONS

The integration of analyses based on field data and numerical simulations has helped to understand scaling mechanisms that might be currently occurring at Nag-67. A review of historical injection records, fluid chemistry data, and analyses of scale materials suggest scaling at Nag-67 occurred mainly in the rock formation immediately adjacent to the wellbore. Sensitivity analyses using reactive transport modeling suggest that the deposition of silica at this location depends primarily on the silica concentration, the temperature, the flow rate, and the pH of the injected brine.

It is possible that the foremost cause of permeability and injectivity loss in the Nag-67 injector is the increased residence time of injected fluid in the well during periods of low or no flow. This potential for increased scaling is being further investigated.

The results of numerical simulation reported here are preliminary. More accurate predictions of injectivity loss would be obtained using a more sensitive coupling of permeability to porosity. Also, the modeling effort could benefit from a more rigorous formulation of silica precipitation kinetics, including a silica nucleation model. Nevertheless, integrating simple numerical simulations as described here, together with semi-quantitative analyses of field data, provided a useful insight into operational constraints and other factors controlling silica deposition around a typical geothermal injection well.

ACKNOWLEDGMENT

This work was supported by Philippine Geothermal, Inc. and the National Power Corporation of the Philippines, and by the Assistant Secretary for Energy Efficiency and Renewable Energy, Office of Wind and Geothermal Technologies, of the U.S. Department of Energy, under Contract No. DE-AC03-76SF00098.

REFERENCES

Carroll, S., Mroczek, E., Alai, M., and Ebert, M. 1998. Amorphous Silica Precipitation (60 to 120°C): Comparison of Laboratory and Field Rates. *Geochimica et Cosmochimica Acta, 62*, (8), 1379-1396.

Gunnarsson, I. and Arnórsson, S., Amorphous Silica Solubility and the Thermodynamic Properties of H_4SiO_4 in the Range of 0º to 350ºC at P_{sat}. *Geochimica et Cosmochimica Acta, 64*, (13), 2295-2307, 2000.

Icopini, G., Brantley, S.L., Heaney, P., Kinetics of silica oligomerization and nanocolloid formation from supersaturated solutions at 25ºC, For submission to *Geochimica et Cosmochimica Acta*, 2003.

Johnson, J.W., Oelkers, E.H., Helgeson, H.C., SUPCRT92: A software package for calculating the standard molal thermodynamic properties of minerals, gases, aqueous species, and reactions from 1 to 5000 bars and 0 to 1000 degrees C. *Computers and Geosciences* 18, 899–947, 1992.

Narasimhan, T.N., Witherspoon, P.A., An integrated finite difference method for analyzing fluid flow in porous media, *Water Resource. Res.* 12, 57–64, 1976.

Pape, H., Clauser C., and Iffland J., Permeability prediction based on fractural pore-space geometry, Geophysics, 64(5), 1447-1460, 1999.

Parkhurst, D.L., Thorstenson, D.C., Plummer, L.N., PHREEQE: A computer program for geochemical calculations: US Geological Survey, Water Resources Investigation 80-96, 174 pp., 1980.

Parks, G.A., 1990. Surface energy and absorption at mineral-water interfaces: an introduction. Rev. Mineral., 23 (Miner.-Water Interface Geochem.), 133-75.

Pruess, K., TOUGH2: A general numerical simulator for multiphase fluid and heat flow, Lawrence Berkeley Laboratory Report LBL-29400, Berkeley, California, 1991.

Reed, M.H., Calculation of multicomponent chemical equilibria and reaction processes in systems involving minerals, gases and aqueous phase. *Geochim. et Cosmochim. Acta* 46, 513-528, 1982.

Santos, S.L., Carandang-Racela, B.D., Injection history and strategy – Tiwi Geothermal Field, Philippines, Proceedings 15th New Zealand Geothermal Workshop, 35-39, 1993.

Spycher N.F., Sonnenthal, E.L., and Apps, J.A., Fluid flow and reactive transport around potential nuclear waste emplacement tunnels at Yucca Mountain, Nevada, *J. Contam. Hydrol*., In press, 2002.

Steefel, C.I., Lasaga, A.C., A coupled model for transport of multiple chemical species and kinetic precipitation/dissolution reactions with applications to reactive flow in single phase hydrothermal system. *Am. J. Sci.* 294, 529-592, 1994.

Vaughan, P.J., Analysis of permeability reduction during flow of heated, aqueous fluid through Westerly Granite, in C.F. Tsang (ed.), Coupled processes associated with nuclear waste repositories, pp. 529-539, Academic Press, New York, 1987.

Verma, A., and K. Pruess, Thermohydrological conditions and silica redistribution near high-level nuclear wastes emplaced in saturated geological formations: *J. Geophys. Res*., 93, 1159-1173, 1988.

Wolery, T.J., EQ3/6: Software package for geochemical modeling of aqueous systems: Package overview and installation guide (version 7.0). Lawrence Livermore National Laboratory Report UCRL-MA-110662 PT I, Livermore, California, 1992.

Xu, T., Pruess, K., Coupled modeling of non-isothermal multiphase flow, solute transport and reactive chemistry in porous and fractured media: 1. Model development and validation. Lawrence Berkeley National Laboratory Report LBNL-42050, Berkeley, California, 38 pp., 1998.

Xu, T., and K. Pruess, Modeling multiphase non-isothermal fluid flow and reactive geochemical transport in variably saturated fractured rocks: 1. Methodology, *Am. J. Sci*., 301, 16-33, 2001.